Potential impacts of climate change on soil erosion vulnerability across the conterminous United States

Citation	Segura, C., Sun, G., McNulty, S., & Zhang, Y. (2014). Potential impacts of climate change on soil erosion vulnerability across the conterminous United States. Journal of Soil and Water Conservation, 69(2), 171-181. doi:10.2489/jswc.69.2.171
DOI	10.2489/jswc.69.2.171
Publisher	Soil and Water Conservation Society
Version	Version of Record
Citable Link	http://hdl.handle.net/1957/47479
Terms of Use	http://cdss.library.oregonstate.edu/sa-termsofuse

doi:10.2489/jswc.69.2.171

Potential impacts of climate change on soil erosion vulnerability across the conterminous United States

C. Segura, G. Sun, S. McNulty, and Y. Zhang

Abstract: Rainfall runoff erosivity (*R*) is one key climate factor that controls water erosion. Quantifying the effects of climate change–induced erosivity change is important for identifying critical regions prone to soil erosion under a changing environment. In this study we first evaluate the changes of *R* from 1970 to 2090 across the United States under nine climate conditions predicted by three general circulation models for three emissions scenarios (A2, A1B, and B1) from the Fourth Assessment Report of the Intergovernmental Panel on Climate Change. Then, we identify watersheds that are most vulnerable to future climate change in terms of soil erosion potential. We develop a novel approach to evaluate future trends of *R* magnitude and variance by incorporating both the rate of change with time as well as the level of agreement between climatic projections. Our results show that mean decadal *R* values would increase with time according to all nine climatic projections considered between 1970 and 2090. However, these trends vary widely spatially. In general, catchments in the northeastern and northwestern United States are characterized by strong increasing trends in *R*, while the trends in the midwestern and southwestern United States are either weak or inconsistent among the nine climatic projections considered. The northeastern and northwestern United States will likely experience a significant increase in annual variability of *R* (i.e., increase in extreme events). Conversely the variability of *R* is unlikely to change in large areas of the Midwest. At the watershed scale (8-digit Hydrologic Unit Code), the mean vulnerability to erosion scores vary between –0.12 and 0.35 with a mean of 0.04. The five hydrologic regions with the highest mean vulnerability to erosion are 5, 6, 2, 1, and 17, with values varying between 0.06 and 0.09. These regions occupy large areas of Ohio, Maryland, Indiana, Vermont, and Illinois, with mean erosion vulnerability score statewide above 0.08. Future watershed management aiming at reducing soil erosion should focus on areas with the highest soil erosion vulnerability identified by this study.

Keywords: climate change—erosivity factor—extreme events—precipitation—Revised Universal Soil Loss Equation—soil erosion

Erosion is the physical process by which soil particles are detached and removed from the ground surface by water or wind. Soil erosion threatens soil fertility due to nutrient and organic matter loss, while also decreasing water quality through increased turbidity (Brown and Froemke 2012). These impacts can reduce food production (Bridges and Oldeman 1999), aquatic life (Waters 1995; Wood and Armitage 1997; Kemp et al. 2011), and the physical stability of fluvial systems. Recent studies suggested that soil erosion and sediment movement have important influences on carbon (C) sequestration potential in soils and ecosystems (Smith et al. 2001; Lal 2005). Therefore, quantifying the impacts of climate change on soil erosion has important implications to the understanding of their environmental impacts as well as the feedbacks of soil C dynamics to global warming. The rate of erosion depends on many factors including precipitation intensity, soil characteristics, topography of the terrain, and land cover type. The complex relationships among these factors and soil erosion are integrated within the Universal Soil Loss Equation (USLE). This empirical model was introduced over 50 years ago (Wischmeier and Smith 1978) and the Revised Universal Soil Loss Equation (RUSLE) was created in the early 1990s (Renard et al. 1991). The RUSLE has been the most widely used model to predict soil erosion (Van Rompaey et al. 2001; Pruski and Nearing 2002; Yang et al. 2003; Angima et al. 2003; Fernandez et al. 2003; Jiang et al. 2012). The USLE/RUSLE equation depends on five factors related to climate (i.e., rainfall runoff erosivity [*R*]), soil type (i.e., erodibility factor [*K*]), topography (i.e., slope steepness and length factor, [*LS*]), land cover type (cover management factor [*C*]), and cultivation management (i.e., conservation practice factor [*CP*]). The first factor is a sole function of rainfall frequency and intensity; both are influenced by climate change.

To our best knowledge, only one conterminous United States (CONUS) scale study analyzed the impact of climate change on soil erosion (Nearing 2001). In that study, an analysis of the spatial changes of *R* based on monthly and annual precipitation predictions by two coupled atmosphere ocean global climate models (GCMs) was conducted. Nearing (2001) found evidence for significant changes in *R* in several regions of the CONUS. Specifically, he found that for the CONUS, the mean percent *R* could increase between 16% and 58% from current (i.e., annual mean between 2000 and 2019) to future (i.e., annual mean between 2080 and 2099) conditions.

The two GCMs used by Nearing (2001) included the Hadley Center Coupled Model, version 3 (HadCM3.1) (Wood et al. 1999; Gordon et al. 2000; Pope et al. 2000) resolved at 2.5° latitude and 3.75° longitude. The predicted precipitation data used by Nearing (2001) corresponded to HadCM3.1 simulations, assuming a 1% increase in greenhouse gases for the study period. The other GCM used by Nearing (2001) was the first gen-

Catalina Segura is an assistant professor in the Forestry Engineering, Resources and Management Department at Oregon State University in Corvallis, Oregon. **Ge Sun** is a research hydrologist for the Eastern Forest Environmental Threat Assessment Center of the USDA Forest Service in Raleigh, North Carolina. **Steve McNulty** is an ecologist and team leader of the Eastern Forest Environmental Threat Assessment Center of the USDA Forest Service in Raleigh, North Carolina. **Yang Zhang** is a professor in the Department of Marine, Earth, and Atmospheric Sciences, North Carolina State University in Raleigh, North Carolina.

eration of the Canadian Center for Climate Modeling and Analysis (CCCma) Coupled Global Climate Model (CGCM1) (Flato et al. 2000). The model resolution is 3.7° × 3.7°. In that study, Nearing (2001) used the precipitation data at the original mentioned spatial resolutions of each GCM.

Yang et al. (2003) attempted to forecast the impacts of climate change on soil erosion on a global scale at a 0.5° spatial resolution. In their study, erosion rates were computed using the RUSLE equation (Renard et al. 1991) for historic, current, and future conditions predicted by GCMs from the Second Assessment Report (AR2) of the Intergovernmental Panel on Climate Change (IPCC). More recently an assessment of future impacts on *R* was conducted for northeast China (Zhang et al. 2010) based on the IPCC Fourth Assessment Report (AR4) monthly precipitation predictions temporally downscaled to daily time series. They forecasted a general increase in erosivity over the region by the mid-21st century with higher changes in *R* for the northern portion of the study area.

Two regional studies have attempted to quantify the impacts of climate change on soil erosion, runoff, and crop productivity in the Changwu region of China (Zhang and Liu 2005; Li et al. 2011). Both studies used downscaled climate data from monthly to daily time steps. The first study considered climatic projections from the HadCM3 model (Wood et al. 1999; Gordon et al. 2000; Pope et al. 2000) between 2070 and 2090 under three emission scenarios, whereas the second considered projections between 2010 and 2039 for four GCMs and three emission scenarios from the Third Assessment Report (AR3) of IPCC (IPCC 2001). The first lacked spatial downscaling providing a regional sensitivity assessment of natural resources to climate change, whereas the second that incorporated spatial downscaling provided a better description of the actual physical processes. Both studies documented changes in precipitation between −2.6% and 37%, changes in soil loss between −5% and 195%, and general tendency for crop production to increase. They also documented that the adoption of the conservation tillage would have great potential to reduce the adverse effects of future climate change. Recent studies have also highlighted that future erosion rates are related to increase frequency of large precipitation events. A study that evaluated the effects of cropping and tillage systems on soil erosion and surface runoff in central Oklahoma (Zhang 2012) established that even though future precipitation (2010 to 2039) is expected to decreases by 6% according four GCMs under three emission scenarios from the AR3 of IPCC (IPCC 2001) the expected average runoff and soil loss will increase by 20% and 44%, respectively. They believe that the increases result from a 12% increase in precipitation variance. The importance of precipitation variance on soil erosion is not limited to croplands. A study conducted in western United States rangelands of Arizona indicated that climate change is expected to impact runoff and soil erosion in this ecosystem as well (Zhang et al. 2012). Their results based on projected climate data for 2050 to 2090 considered seven GCMs under three emission scenarios suggested no significant changes in annual precipitation compared to the historic period 1970 to 1999 across the region, while projected mean annual runoff and soil loss increased significantly, ranging from 79% to 92% and from 127% to 157%, respectively. The dramatic increases in runoff and soil loss were attributed to the increase in the frequency and intensity of extreme events in the study area.

In this study, we conduct an assessment of the vulnerable areas to erosion under future climatic projections. The objectives of this study are to (1) evaluate the temporal and spatial changes of *R* from 1970 to 2090 across the CONUS under multiple climate change projections and (2) identify the spatial distribution of areas most vulnerable to soil erosion. The ultimate goal of this study is to provide guidance to land managers who direct resources in soil erosion control and watershed restoration efforts in response to climate change.

Approach

The study area corresponds to the CONUS and the time frame of 1970 to 2090. The spatial resolution of each dataset used in this investigation varies between 30 × 30 m (98 × 98 ft) grid to eight-digit hydrologic units (HUC-8 watersheds) defined by the US Geological Survey (USGS). Soil and digital elevation model (DEM) data are available at 90 × 90 m (295 × 295 ft) grid resolution (Wolock 1997; Jarvis et al. 2006). Although higher resolution (30 × 30 m [98 × 98 ft]) data are available for a DEM (Abrams 2000), studies suggested that there are no significant differences in terms of calculated slopes between the two datasets (R. Bhattarai, personal communication, September 2012). The land cover data are available at a grid resolution of 30 × 30 m (98 × 98 ft) (Fry et al. 2011), and the precipitation data between 1966 and 2095 (Maurer et al. 2007; Meehl et al. 2007) are rescaled to the HUC-8 watershed scale (Caldwell et al. 2012).

Climate Data. In this study, we consider monthly precipitation data predicted by three GCMs under three emission projections of greenhouse gases: low (B1), intermediate (A1B), and high (A2), from the AR4 of the IPCC (Trenberth et al. 2007). The three GCMs under three emission scenarios provide a total of nine possible future precipitation projections. Monthly and annual precipitation estimates archived under these different climatic projections were downscaled and biased corrected by others from their original grid resolutions to a resolution of 12 × 12 km (7.5 × 7.5 mi). This dataset is known as the bias corrected and downscaled World Climate Research Programme's (WCRP) Coupled Model Intercomparison Project phase 3 (CMIP3) Climate Projections (Maurer et al. 2007; Meehl et al. 2007). This data set includes both the 20th century observational surface climate conditions (Maurer et al. 2007) and each GCM's 21st century climate simulation. Our analysis considers computed weighted mean precipitation data to 2,099 HUC-8 across the CONUS (Caldwell et al. 2012) with varying drainage areas between 184 km^2 (114 mi^2) and 23,000 km^2 (14,292 mi^2), with an average of 3,751 km^2 (2,331 mi^2). We preferred using climatic data at the HUC-8 watershed resolution rather than the 12 km (7.5 mi) grid because these hydrologic units are commonly used in the context of water resources management. HUC-8 watersheds are the common resolution used at the CONUS scale in other studies that examine future urbanization, hydrologic and ecosystems modeling, air and water quality linkage, and water supply stress (Liang et al. 2002; Sun et al. 2008; Theobald et al. 2009; Schwede et al. 2009; Sun et al. 2011; Caldwell et al. 2012).

The updated precipitation predictions by these GCMs (table 1) should result in a more realistic assessment of the potential effects of climate change on erosivity. We consider the predictions of the 3rd generation CGCM3.1 model at a spatial resolution of

Table 1
Global climate model (GCM) used in this study.

GCM	Organization	Model resolution (latitude × longitude)	References
HadCM3	Hadley Climate Research Center, United Kingdom	2.5° × 3.75°	Wood et al. 1999; Gordon et al. 2000; Pope et al. 2000
CGCM3	Canadian Center for Climate Modeling and Analysis, Canada	3.7° × 3.7°	Flato and Hibler 1992; Flato and Boer 2001; Kim et al. 2002; Kim et al. 2003
CM2	Geophysical Fluid Dynamics Laboratory, United States	2.0° × 2.5°	Delworth et al. 2006; Gnanadesikan et al. 2006; Stouffer et al. 2006; Wittenberg et al. 2006

3.7°. This GCM uses the same ocean component as that used in the second generation model, which incorporated an isopycnal/eddy stirring parameterization (Gent and McWilliams 1990) as well as sea-ice dynamics (Flato and Hibler 1992). This version 3.1 makes use of updated atmospheric ocean components (Flato and Boer 2001; Kim et al. 2002; Kim et al. 2003). The second GCM used is the Geophysical Fluid Dynamics Laboratory Coupled Model (CM), version 2.0 (Delworth et al. 2006; Gnanadesikan et al. 2006; Stouffer et al. 2006; Wittenberg et al. 2006). This is a coupled GCM with a spatial resolution of 2.0° latitude × 2.5° longitude (corresponding approximately 222 × 213 km [138 × 132 mi] at 40° latitude). The atmospheric components include representations of radioactive fluxes, mixing in the atmospheric boundary layer, impacts of clouds, drag on upper level winds, changes in the spatial distribution of ozone, and the impact of multiple greenhouse gases. The last GCM considered corresponds to the same HadCM3.1 used by Nearing (2001), which has been used in both AR3 and AR4 of the IPCC, and allows for direct comparison between the two studies.

Soil Erodibility. Soil erodibility (*K*), is one of the variables in USLE (Wischmeier and Smith 1978) and its revised version, RUSLE (Renard et al. 1991). Soil erodibility represents the inherent erodibility of a given soil. Soil erodibility values for the CONUS vary between 0.04 and 0.64 with a mean value of 0.26 ± 0.09 (Wolock 1997). Soils rich in sand and clay are characterized by low *K* values whereas high values of *K* are common in soils with high silt content (Wischmeier and Smith 1978; Renard et al. 1991). Values of *K* are reported at 1 × 1 km (0.62 × 0.62 mi) grid resolution by the USGS (Wolock 1997). According to this information, large areas in the Midwest (i.e., Illinois, Indiana, Wisconsin, Iowa, Missouri, Kansas, Tennessee, and Nebraska) are characterized by high values of *K* (above 0.35). Conversely, high-elevated areas in the west where rock outcrops are common are cauterized by very low *K* values (<0.16).

Topography. Topographic slope in percentage is derived for the CONUS based on a 90 × 90 m (295 × 295 ft) DEM (Jarvis et al. 2006) within ArcGIS 10. Mountainous regions in the west and the Appalachians in the east have the highest values of slope across the country.

Land Use and Land Cover. Land cover data at 30 × 30 m (98.4 × 98.4 ft) grid resolution from 2006 are used in this investigation (Fry et al. 2011). This raster dataset includes 16 land cover categories dominated by forest (25%), shrub and scrub (21%), and cultivated crops (16%). The spatial distribution of these categories is assumed to remain constant over time even though we recognize that land cover is likely to change in the future. While general patterns of land use change may be understood, the specific locations of that change are very difficult to predict. We resample this raster to a 90 × 90 m (295 × 295 ft) resolution to enable geo-processing across slope and erodibility factors.

Estimation of Rainfall-Runoff Erosivity. The *R* factor can be directly calculated with a simple mathematical expression as a function of maximum 30-minute rainfall intensity (I_{30}) and total storm kinetic energy (*E*) for multiple years (Wischmeier and Smith 1978). However, hourly data for calculating *R* are not available for many locations in the CONUS and they are not yet available for any future climate predictions. The alternative to hourly data to compute *R* is using empirical relations based on monthly or annual estimates of future precipitation. These empirical methods are crude because they fail to fully reflect possible *R* changes due to the increases in large extreme rainfall events, which is one of the most significant aspects of future climate change. Several empirical relations have been developed for different geographic regions. Early efforts established strong relations between *R* and annual precipitation in West Africa (from Cameroon to Senegal), Zimbabwe, and Hawaii (Stocking and Elwell 1976; Roose 1977; Lo et al. 1985). For the CONUS similar relations were developed based on data from 132 locations (Renard and Freimund 1994). Likewise other relations have been established for Australia, Europe, Central and South America, and Asia (Bolinne et al. 1980; Mikhailova et al. 1997; Millward and Mersey 1999; Sepaskhah and Sarkhosh 2005; Bonilla and Vidal 2011). Empirical relations to estimate *R* based on monthly precipitation data have also been established since the mid-1970s by Arnoldus (1977) for stations in Morocco and the CONUS. That work was followed by others (Renard and Freimund 1994; Ferro and Porto 1999; Loureiro and Coutinho 2001; Nearing 2001; Irvem et al. 2007; Andrade et al. 2010; Ozsoy et al. 2012) working in the CONUS, Portugal, Australia, Turkey, Italy, and Venezuela. We estimate *R* using equations derived for the CONUS by Renard and Freimund (1994) based on monthly precipitation. We prefer the estimates based on the monthly rather than annual data because the former captures intraannual variability:

$$F = \frac{\sum_{i=1}^{12} P_i^2}{P}, \quad (1)$$

$$R = 0.7397F^{1.847}, \text{and} \quad (2)$$

$$R = 95.77 - 6.081\text{F} + 0.0477F^2, \quad (3)$$

where *F* is a Fournier coefficient (Arnoldus 1977; Arnoldus 1980), P_i (mm) is the total monthly precipitation, and *P* (mm) is the total annual precipitation. The units of *R* are expressed as MJ mm ha^{-1} y^{-1}. Equation 2 is recommended for *F* <55 mm (2 in) and equation 3 is recommended for *F* >55 mm (2 in) (Renard and Freimund 1994). These equations were also chosen in other large scale assessment of *R* (Nearing 2001; Yang et al. 2003; Oliveira et al. 2012).

Annual estimates of R between 1966 and 2095 are calculated for every HUC-8 watershed using equations 1 through 3. Then 13 decadal averages between 1970 and 2090 are computed for 9 climate projections independently (i.e., 13 decadal averages per climate projection per HUC-8 watershed). Renard and Freimund (1994) found limitations with their empirical model as equations 2 and 3 are not appropriate for areas with high winter precipitation located in mountainous areas and in western Washington, Oregon, and northwestern California. They found that all these sites also have high mean annual precipitation (>800 mm [31 in]) and $F >$ 100 mm (4 in) (equation 1).

Temporal Trends in Rainfall Runoff Erosivity Factor. The decadal R values computed per HUC-8 watershed are analyzed in order to identify the areas in which R is likely to change under future climate. The linear relation between mean decadal values of R and time are evaluated for each climate projection on each HUC-8 watershed. The likelihood of change in R (expressed as CR) as assessed by combining the nine individual slopes of the aforementioned regressions:

$$CR = \frac{\langle m \rangle}{\langle \sigma_m \rangle}, \quad (4)$$

where, $\langle m \rangle$ and $\langle \sigma_m \rangle$ are the mean and standard deviation (std) of the slopes of the nine linear relations. This value can theoretically vary between $-\infty$ and ∞. Table 2 provides the range of CR considered and the corresponding scores along with their interpretation. A value of $CR >5$ indicates that $\langle m \rangle$ is positive and more than five times the mean standard deviation of the slope. Thus there is a strong statistical indication that most models agree and predict an increase in the R. Likewise a value of $CR <5$ provides a strong indication that R will decrease in the future. CR values between -5 and -3 and between 3 and 5 are assumed to indicate a decrease or increase, respectively, with less statistical strength and values of CR between -3 and 3 indicate no clear trend of change of R.

An additional analysis is performed to determine if the interannual variability of R (i.e., std, σ_r, around decadal mean values of R) will change in the future. We compute the slope s of the relation between time and std σ_r for each climatic projection in each HUC-8 watershed. Similarly to the relation between R and time (equation 4), we compute a metric, CS, to qualify the likelihood of change in the temporal variability of σ_r:

$$CS = \frac{\langle s \rangle}{\langle \sigma_s \rangle}, \quad (5)$$

where $\langle s \rangle$ and $\langle \sigma_s \rangle$ are the average and std of the slopes of the nine linear relations between σ_r and time. The range of CR considered and the corresponding scores are presented in table 2. The spatial distributions of the scores for CR and CS are mapped, converted into a 90 m (295 ft) grid, and use directly to compute vulnerability to erosion with the other three factors considered to identify vulnerable areas to erosion.

Table 2
Statistical criterion to establish temporal change in erosivity magnitude (*CR*) and variance considering nine climatic scenarios (*CS*). *CR* and *CS* are described by equations 4 and 5.

CR or CS	Score (*CR* and *CS*)	Interpretation
<–5	–1	*R* or variance of *R* is very likely to decrease
–5 to –3	–0.5	*R* or variance of *R* is likely to decrease
–3 to 3	0	No clear trend in *R* or variance of *R*
3 to 5	0.5	*R* or variance of *R* is likely to increase
>5	1	*R* or variance of *R* is very likely to increase

Identification of Areas Vulnerable to Erosion. In this study, four out of the five influential factors that control soil erosion according to the RUSLE equation (Renard et al. 1991) are taken into account directly (R, K) or indirectly (LS, C). In the case of R we scale the scores CR and CS (equations 4 and 5) to vary between –1 and 1 (see table 2). The other three factors (erodibility, slope, and land cover) are scaled to vary between 0.25 and 1 (table 3). The scores given to erodibility divide the range into four categories with similar spatial expend (23% to 28% of the CONUS is classified into each of the four categories, table 3). In the case of LS, only slope (S) was considered because the length factor (L) is basically constant and equal to the DEM resolution (90 m [295 ft]). The S categories are identified ensuring that the scheme is efficient at highlighting the mountainous areas of the country. These categories give a minimum value of 0.25 to areas with slope less than 1% (36% of the CONUS), a score of 0.5 to areas with a slope between 1% and 5% (28% of the CONUS), a score of 0.75 to areas with slope between 5% and 10% (17% of the CONUS), and a score of one for areas with slopes above 10% (19% of the CONUS). In the case of land cover (LC), only two categories are considered to highlight the high vulnerability to erosion of croplands compare to all other land cover type (table 3). We incorporate the effect of each factor (e.g., R, K, S, and LC) by classifying each 90 m (295 ft) grid cell into the mention categories. The CP factor of the RUSLE equation is not considered here, as it is largely for agricultural erosion assessments which are beyond the scope of this work.

The scores given to R (CR and CS) represent climate as the driving force of the erosion process. We give the same weight to each of these in the scheme because both changes in the magnitude and variance of R are likely to cause changes in the vulnerability to erosion (equation 6). The remaining three factors, K, S, and LC are all given the same weight (i.e., multiply together). Our objective is not to compute actual values of erosion but to conduct a qualitative assessment of the most vulnerable areas to this process. All the geo-processing was conducted under ArcGIS 10.0 to produce a map of areas vulnerable to erosion (E):

$$E = \frac{CR+CS}{2} \times S \times K \times LC \ , \quad (6)$$

where E can vary between –1 and 1. When land cover and soil erodibility are not considered, an intermediate map produced in this scheme as the product of R (average CR and CS) and S provides an approximate assessment of the vulnerable areas to mass wasting processes mainly driven by rainfall (R) and gravity (S). The values for mass wasting hazard can also vary between –1 and 1.

Outcomes

Spatial and Temporal Trends of Rainfall Runoff Erosivity (R). The CONUS mean decadal erosivity values, R, vary between 5,227 and 8,639 MJ mm ha^{-1} y^{-1} between 1970 and 2090. These average values increase with time according to all nine models considered (figure 1). However, these trends vary widely spatially when compared among individual watersheds (figure 2). In general, catchments in the northeastern and north-

western United States are characterized by strong increasing trends in *R* (i.e., areas in red in the map, figure 2a) while the trends in the midwestern and southwestern United States are either weak or contradictory among models (i.e., areas in white in the map, figure 2a). There are only 71 watersheds (3.4%), located mainly in Colorado and Kansas, in which most climatic scenarios indicate that *R* will decrease in the future (i.e., areas in blue, figure 2a). Considering the limitations highlighted by Renard and Freimund (1994) about the applicability of equations 2 and 3, we identified 124 HUCs in which these equations are inappropriate in at least one year for at least one climactic projection between 1961 and 2099. These watersheds are located mainly in western Washington, Oregon, and California (figure 2).

The mean value of *R* considering all nine climatic projections between the historic period of 1970 and 2010 differ significantly from those between the future period of 2050 and 2090 (probability <0.05) in 1,630 basins mainly located in the northeastern and northwestern United States (figure 2b). The change is positive (i.e., increase in *R*) in most cases (91%). The mean percentage change in *R* in these basins is 20.2% ± 33% and varies between –66.7% and 398% (figure 2b). The analysis of interannual variability of *R* indicates that the northeastern United States, along with large areas in both the northwestern and southeastern United State regions will likely experience a significant increase in the std of the mean decadal *R* values (figure 2c). Conversely, the variability of *R* is unlikely to change in large areas of the Midwest. This finding indicates that water and soil resources management strategies for the northern regions would require a higher degree of adaptability than that for other regions in the country.

Our assessment of future *R* values provides an improved effort presented by Nearing (2001). Similarly to Nearing (2001) findings, our study shows that *R* is likely to increase in the future in large areas to the country. Nearing (2001) found a clear increase in *R* for New England and the Mid-Atlantic states north from Georgia. Conversely, Nearing (2001) results were very divergent for the southwestern region and to a lesser extent for the southeastern states. Our methodology incorporates simultaneously the precipitation predictions by more recent climatic projections and therefore offers new and robust information to water and soil managers. Our results are presented at different scales ranging from 90 × 90 m (295 × 295 ft) pixels, to HUC-8 watersheds, to hydrologic regions to facilitate their use and dissemination.

Spatial Distribution in Erodibility, Slope, and Land Cover. The spatial distribution of the scores given to erodibility, slope, and land cover are shown in figure 3. Red areas in the three maps of this figure highlight the most vulnerable areas according to each of the three factors. Areas in the Midwest occupying large portions of Kansas, Oklahoma, North Dakota, South Dakota, Iowa, Illinois, Indiana, and Missouri appear to be vulnerable to erosion according to both land cover (i.e., cultivated crops) and erodibility (i.e., soils rich in silt). The percentage of the area in the CONUS covered with crops is 16% whereas the percentage of the area in the CONUS with *K* values above 0.33 is 25.4%. The spatial correlation between land cover and *K* is expected given that fertile soils (e.g., mollisols) are often characterized by silty textures and therefore high values of *K*. The mean *K* value across the CONUS of 0.26 is lower than the mean value of 0.32 for cultivate crops.

Steep terrain (slope >10%) is common in mountainous regions of Washington, Oregon, Idaho, California, Nevada, Montana, Wyoming, Utah, Colorado, New Mexico, Arizona, Virginia, West Virginia, and North

Table 3
Scores between 0 and 1 assigned to erodibility, slope, and land cover categories for spatial analysis of vulnerable areas to mass wasting and erosion.

Erodibility	Slope (%)	Land cover	Score
>0.33	>10	Cultivated crops	1
0.28 to 0.33	5 to 10	*	0.75
0.20 to 0.28	1 to 5	*	0.5
<0.20	<1	Everything else	0.25

*Cultivated crops are considered more vulnerable than any other land cover types. Thus only two scores (1 and 0.25) are considered.

Figure 1
Mean nationwide decadal values of rainfall runoff erosivity (*R*) between 1970 and 2090 according to nine climatic scenarios.

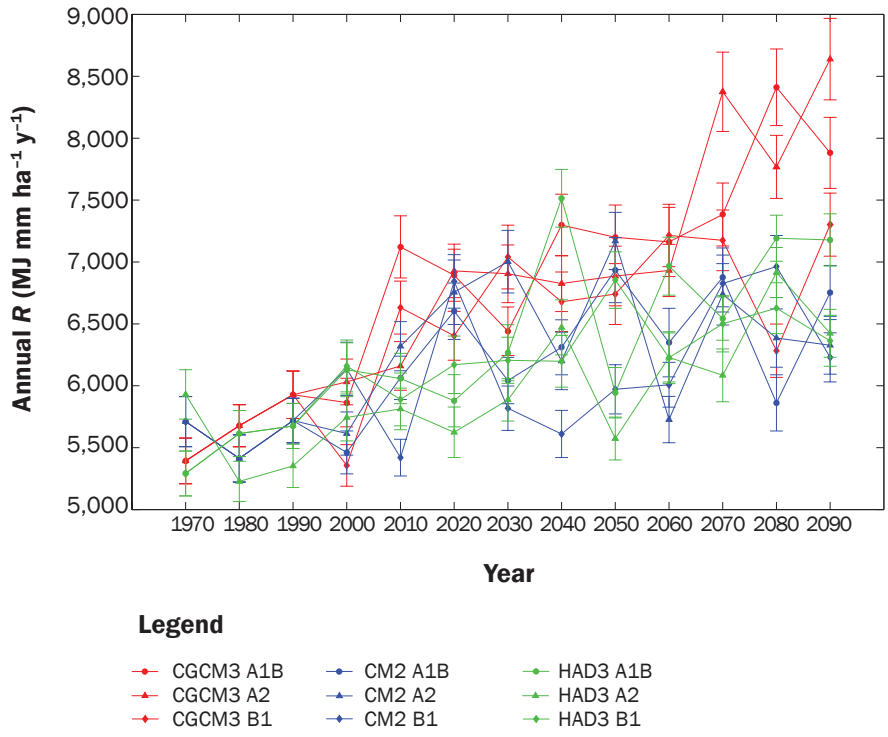

Figure 2
Spatial trends in (a) the likelihood of erosivity to change in the future (table 2), (b) the percentage increase in mean erosivity between 1970 to 2010 and 2050 to 2090, and (c) the likelihood of change in the interannual variability of erosivity.

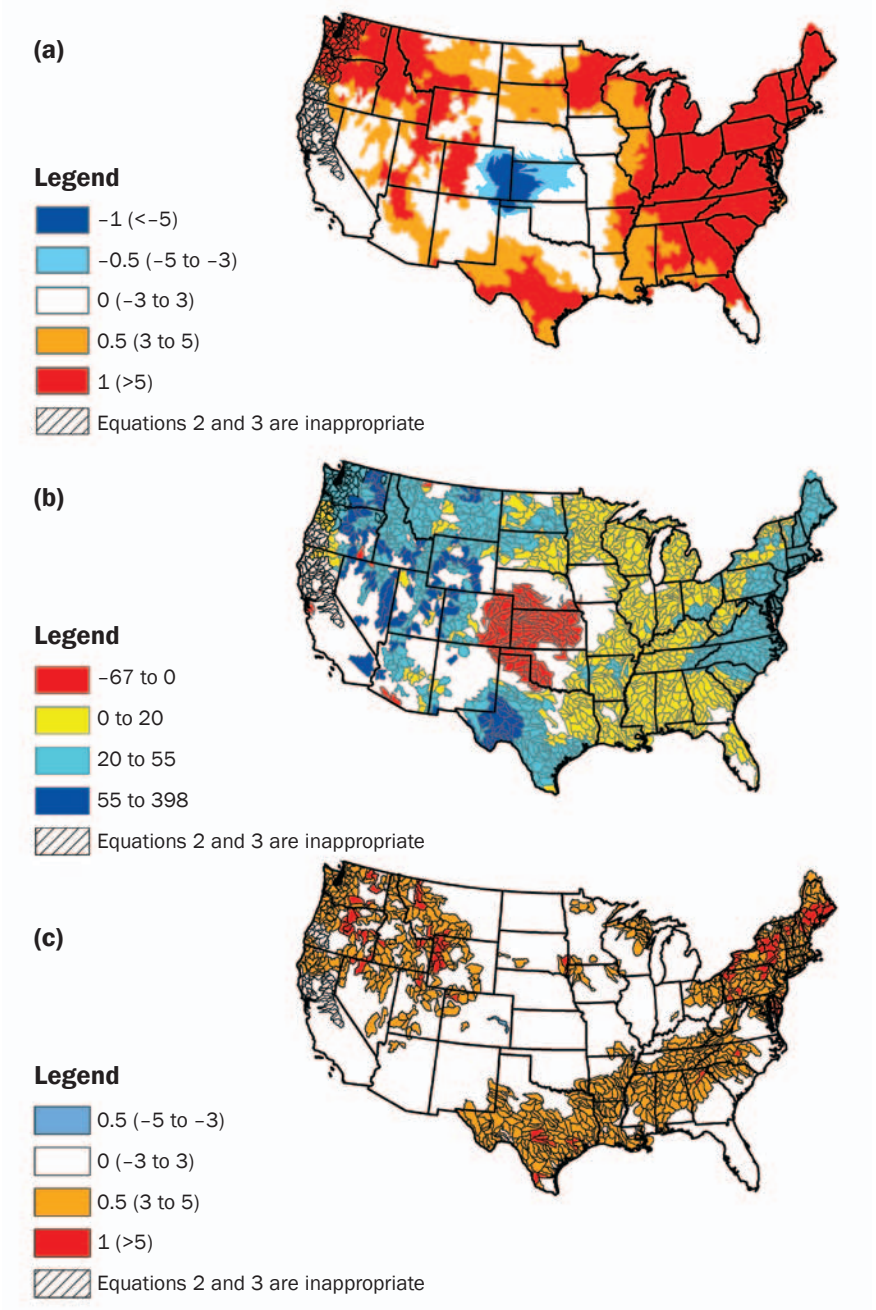

Carolina and occupies 19% of the CONUS. These steep areas are characterized by low values of *K* (figure 3) with a mean *K* of 0.20. As can be expected, cultivated crops occupied a very small portion of these steep areas (i.e., 0.06 %).

Areas Vulnerable to Mass Wasting. The vulnerability to erosion is calculated by considering erosivity (*CR* and *CS*), slope, erodibility, and land cover. An intermediate step in this process corresponding to the spatial distribution of the product of the first two factors provides an approximate assessment of the CONUS vulnerability to mass wasting processes. The mean vulnerability to mass wasting at the pixel scale is 0.21 including all pixels and 0.27 excluding areas with score zero (figure 4). Most of the CONUS reveal scores between 0.12 and 0.37 (50%), whereas 23% of the CONUS have a score of zero (i.e., white areas in figure 4). These areas have a score of zero for (CR + CS) ÷ 2. This assumes that less moisture availability in the soil (i.e., decreased of precipitation) or decreased variability of it results in a decrease of mass movement hazards. This is true most of time regardless of texture. The areas that would experience the highest increase in mass wasting processes (i.e., scores > 1) occupy 0.8% of the CONUS; they are mainly located in mountainous regions of Washington, Oregon, Montana, Wyoming, Maine, and New York. The mean values per HUC-8 watershed vary between –0.3 and 0.96, with a mean among them of 0.22 (figure 5). The watersheds with the highest scores are located along the Appalachian Mountains in the east side of the country and in the Northwest over part of the Cascades Range (figure 5a). Among the 18 hydrologic regions of the CONUS, regions 6, 17, 1, 2, and 5 have the highest mean mass wasting vulnerability scores between 0.36 and 0.5 (figure 5b). These regions include large areas over Vermont, New Hampshire, Washington, Pennsylvania, New York, and Maine with statewide mean values between 0.45 and 0.58 (figure 4). The mean score for Region 11 is negative (–0.001) and highlights the fact that the precipitation projections for most of the HUC-8 watersheds in this region predict a decrease in magnitude and variance in the future and therefore a decrease in *R*. According to our scheme, a consistent decrease in *R* (both magnitude and variance) receives a negative score (blue areas in figures 2a and 5a).

Vulnerable Areas to Erosion. At the 90 m (295 ft) pixel scale, vulnerability to erosion varies between –0.56 and 1 with a mean of 0.04 including all pixels, and of 0.05 excluding areas with zero score (covering 23% of the total area). The most frequent erosion scores across the CONUS vary between 0.03 and 0.25 (49% of the pixels). There are very few CONUS pixels with the maximum possible score of 1 (i.e., < 0.002% of total area) and these areas are limited to steep cultivated areas in Washington, Oregon, Idaho, and New York. High erosion scores (i.e., above 0.5) occupy 0.13% of the CONUS (figure 4) mainly over Washington, Oregon, Idaho, Montana, Ohio, Pennsylvania, New York,

Figure 3
Spatial distributions of the scores given to (a) erodibility (K), (b) slope (S), and (c) land cover (see table 3 for scoring details).

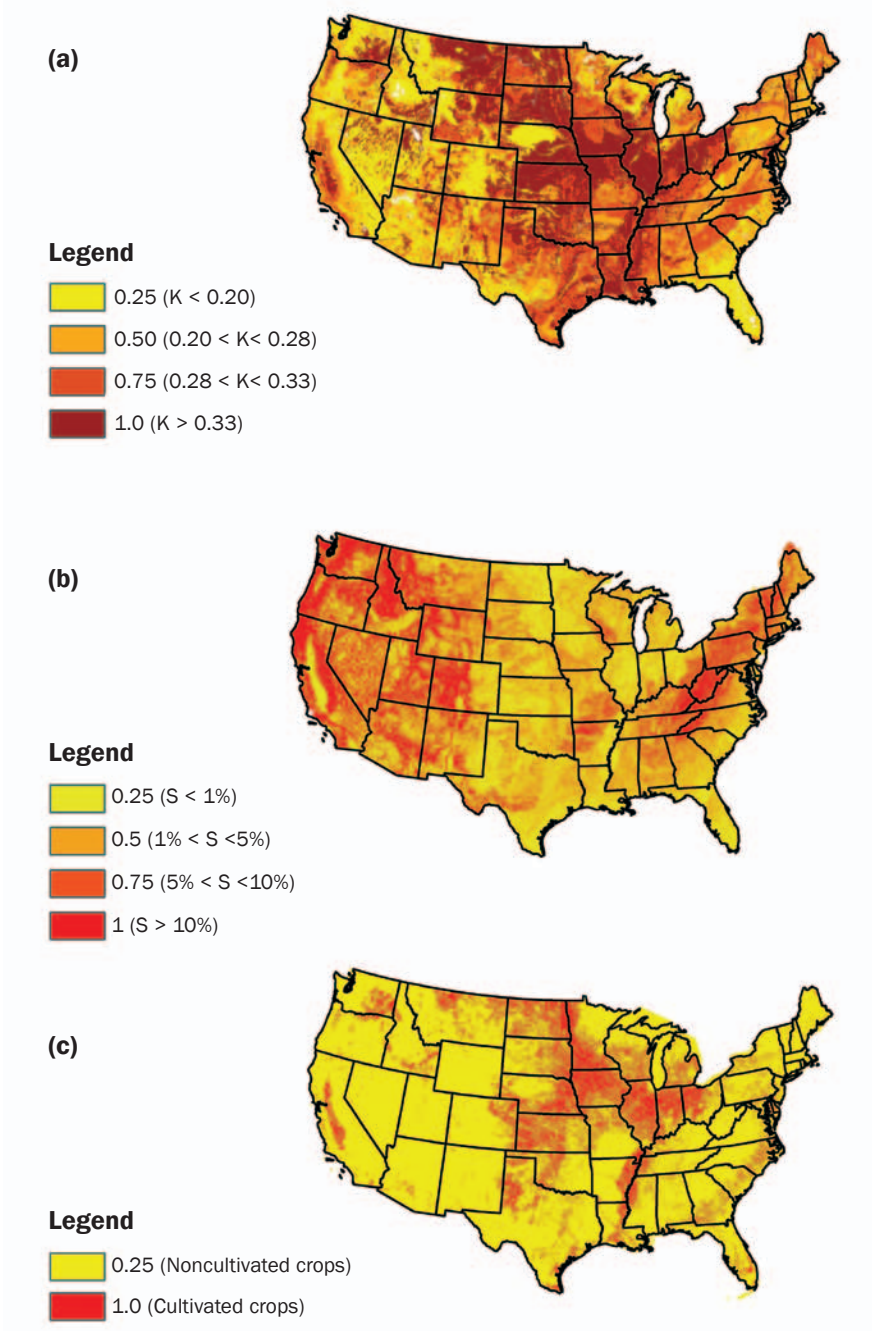

Maryland, and Vermont. At the HUC-8 watershed scale, the mean vulnerability scores vary between –0.12 and 0.35 with a mean of 0.04 (figure 6). The five hydrologic regions with the highest mean vulnerability are 5, 6, 2, 1, and 17 with values between 0.06 and 0.09. These regions expand across Ohio, Vermont, Indiana, Maryland, and Illinois with statewide mean values between 0.08 and 0.12 (figure 6). As in the case of the vulnerable areas to mass wasting, Region 11 has a negative score for vulnerability to erosion (–0.007) due to negative trends in precipitation magnitude and variance over time predicted by most climatic projections considered.

Limitation of Assessment Methods. Our assessment of erosion is qualitative and even though we attempt a more realistic assessment by incorporating recent GCMs, no climatic predictions are available at a high temporal resolution (e.g., hourly precipitation) that would enable better assessment of erosivity. Our approach offers a qualitative assessment of vulnerability to erosion rather than a quantitative calculation of erosion rates. This is an important distinction with respect to the previous CONUS scale assessment of *R* (Nearing 2001). We employ a scheme to incorporate precipitation predictions by different GCMs and emission scenarios in which both the level of agreement between predictions, their magnitudes, and variance are considered. In addition, we consider the effects of other factors such as topography, soil erodibility, and land cover. Our assessment assumes constant land cover over time. This is obviously an unrealistic assumption that adds some level of uncertainty to our results. However, generally speaking the land cover type associated to high erosion is cultivated crops and is not expected to change dramatically over time. Comparisons between spatial land cover data from 2000 and 2006 indicate a percentage change in cultivated crops across the CONUS of less than 0.5%. Higher rates of land cover conversion to crops have been reported at some locations. A recent study indicated land cover change from grasslands to crops of 1% to 5.4 % per year in North Dakota, South Dakota, Nebraska, Minnesota, and Iowa between 2006 to 2011 (Wright and Wimberly 2013). The mean cultivated crop cover in these states varies between 26% and 67% (Fry et al. 2011). According to our results, South Dakota, North Dakota, and Minnesota are more vulnerable than Nebraska and Iowa because *CR* and *CS* are often zero in the latter two. Our static assumption of land cover type also neglects possible plant growth rates changes due to changes in precipitation, temperature, and carbon dioxide patterns in the future. This study provides crucial spatially resolved information that can provide the scientific basis to the development of effective management strategies to mitigate the impacts of climate change.

Summary and Conclusions

There is good agreement among the scientific community that extreme climate in terms of both temperature and rainfall intensity is

Figure 4
Spatial distributions of (a) vulnerability to mass wasting hazard (i.e., [*CR*+*CS*] ÷ 2 × *S*), and (b) vulnerability to erosion (i.e., [*CR*+*CS*] ÷ 2 × *K* × *S* × *LC*).

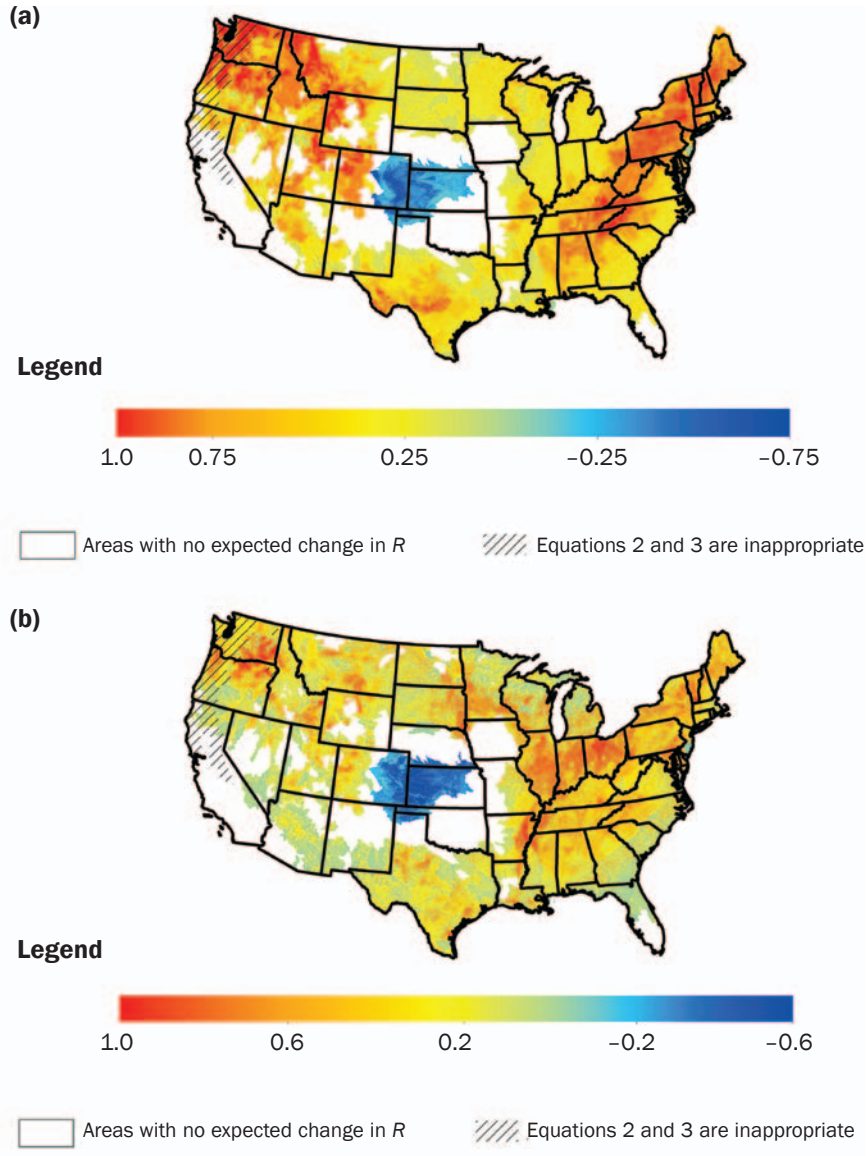

occurring due to global climate warming. While there is little doubt that temperature will continue to rise in the future, there is less agreement in terms of changes in precipitation patterns. Thus, the profound effects of future climate change on ecosystems and human societies are difficult to predict. The results presented here provide an updated analysis of the effects of climate change on soil erosion over the CONUS. Our analyses are based on nine climate projections from three GCMs under three emissions scenarios. Our results show that mean decadal erosivity values for the CONUS between 1970 and 2090 will increase with time according to all nine climatic projections considered. We also found a strong statistical indication that the expected changes in *R*, both in terms of magnitude and variance, vary widely spatially. Most of the northeastern and northwestern US states are characterized by strong increasing trends in *R*. Conversely the trends in the Midwest and Southwest are either weak or contradictory among predictions under the nine climate projections.

The accuracy on our assessment of *R* is limited to both the accuracy of the precipitation projections and the effectiveness of the method employed to compute it. Precipitation projections by different models and emission scenarios provide, in many cases, divergent projections of future climate. However, we believe that our scheme captures efficiently both the rate of change in *R* with time and the degree of agreement between climatic projections. Our approach is not limited to study of individual climatic projections but of their level of agreement measured with a robust statistical quantity. In terms of the methodology employed to compute *R*, we recognize that it is a limitation because *R* is computed based on an empirical equation using monthly precipitation data. However, available GCMs do not offer precipitation data resolved at a higher temporal scale. An evaluation of the accuracy and efficiency of the equation used here to compute *R* would require a comparison between *R* estimates based on precipitation data at different temporal resolutions.

Location and extent of areas vulnerable to soil erosion are computed considering rainfall runoff erosivity (both future change in magnitude and variance), soil erodibility, land cover, and slope. Areas with the maximum vulnerability to erosion are limited to very small portions of Washington, Oregon, Idaho, and New York. These areas are covered by agriculture crops with soils susceptible to erosion (e.g., silty loams) and landscapes with steep terrain (i.e., slope > 10%) and have a clear statistical indication that *R* magnitude and variance will likely increase in the future. The most frequent erosion scores across the CONUS are below 0.1. Conversely high erosion scores > 0.5 occupy only 0.13% of the CONUS and are located mainly in Oregon, Idaho, Montana, Ohio, Pennsylvania, New York, Maryland, and Vermont. The mean vulnerability scores per HUC-8 watershed indicate that the hydrologic regions 5, 6, 2, 1, and 17 over large areas of Ohio, Vermont, Indiana, Maryland, and Illinois will experience the highest mean vulnerability to erosion.

Nonpoint source pollution from soil erosion of agricultural lands is the top cause of water quality problems in the United States. However, soil erosion control is costly, and the associated nonpoint source pollution to rural watersheds is difficult to manage. This study shows that some areas with historic problems of soil erosion will likely continue to have as much or worse soil erosion in the future. Resources of soil conservation must give priorities to those regions identified by this study.

Figure 5
Mean vulnerability to mass wasting by (a) eight-digit hydrologic unit code watershed scale and (b) hydrologic region.

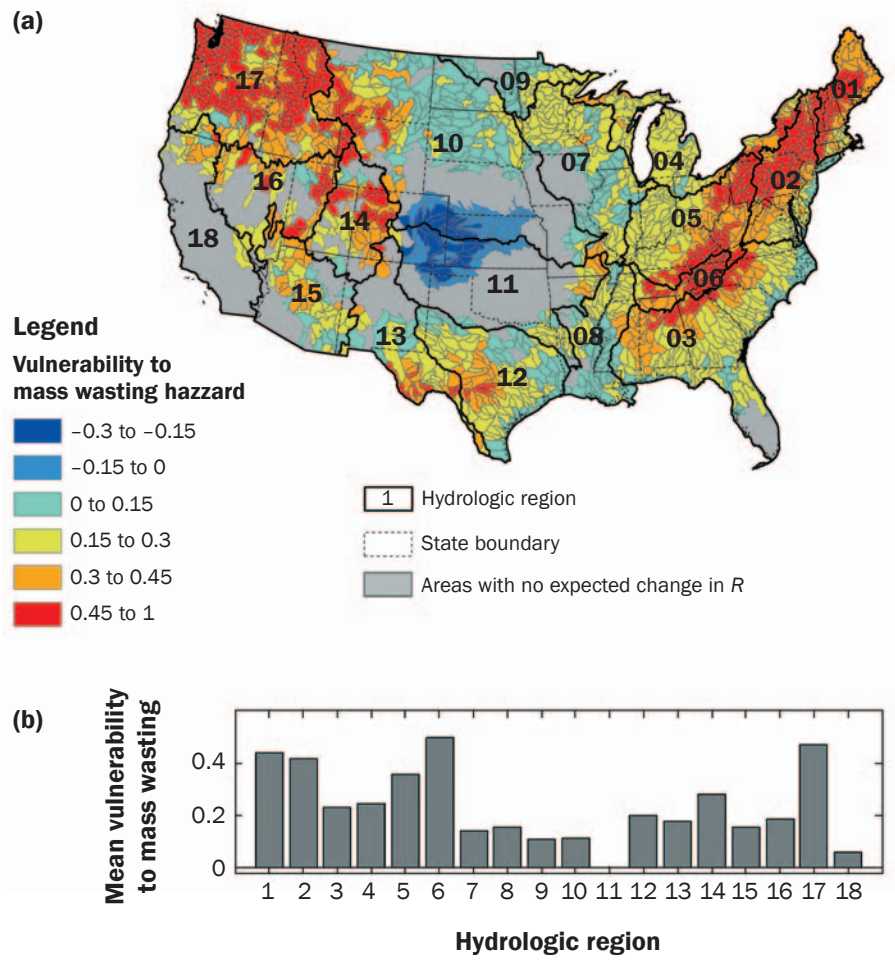

Acknowledgements

This study is funded by the National Science Foundation EaSM program (AGS-1049200) at North Carolina State University. Partial support was provided by USDA Forest Service Eastern Environmental Threat Assessment Center in Raleigh, North Carolina. We also thank Peter Caldwell with the USDA Forest Service, Jeremy Freimund with the Lummi Natural Resources Department for useful discussions, and Erika Cohen and Jennifer Moore Myers with the USDA Forest Service for help with geographic information systems processing. Finally, we would like to thank two anonymous reviewers for providing insightful suggestions.

References

Abrams, M. 2000. The Advanced Spaceborne Thermal Emission and Reflection Radiometer (ASTER): data products for the high spatial resolution imager on NASA's Terra platform. International Journal of Remote Sensing 21(5):847-859.

Andrade, O., M. Kappas, and S. Erasmi. 2010. Assessment of Erosion Hazard in Torres Municipality of Lara State (Venezuela) Based on Gis. Interciencia 35(5):349-356.

Angima, S.D., D.E. Stott, M.K. O'Neill, C.K. Ong, and G.A. Weesies. 2003. Soil erosion prediction using RUSLE for central Kenyan highland conditions. Agriculture Ecosystems & Environment 97(1-3):295-308.

Arnoldus, H. 1980. An approximation of the rainfall factor in the Universal Soil Loss Equation. *In* Assessment of Erosion, eds. M. DeBoodt and D. Gabriels, 127-132. Chichester: John Wiley & Sons.

Arnoldus, H. 1977. Methodology used to determine the maximum potential average annual soil loss due to sheet and rill erosion in Morocco. Food and Agriculture Organization Soils Bulletin 34:39-51.

Bolinne, A., A. Laurant, and P. Rosseau. 1980. Provisional rain-erosivity map of Belgium. *In* Assessment of Erosion, eds. M. Boodt and D. Gabriels, 111-120. Chichester: John Wiley & Sons.

Bonilla, C.A., and K.L. Vidal. 2011. Rainfall erosivity in Central Chile. Journal of Hydrology 410(1-2):126-133.

Bridges, E.M., and L.R. Oldeman. 1999. Global assessment of human-induced soil degradation. Arid Soil Research and Rehabilitation 13(4):319-325.

Brown, T.C., and P. Froemke. 2012. Nationwide assessment of nonpoint source threats to water quality. Bioscience 62(2):136-146.

Caldwell, P.V., G. Sun, S.G. McNulty, E.C. Cohen, and J.A. Moore Myers. 2012. Impacts of impervious cover, water withdrawals, and climate change on river flows in the conterminous US. Hydrology and Earth System Sciences 16(8):2839-2857.

Delworth, T.L., A.J. Broccoli, A. Rosati, R.J. Stouffer, V. Balaji, J.A. Beesley, W.F. Cooke, K.W. Dixon, J. Dunne, K.A. Dunne, J.W. Durachta, K.L. Findell, P. Ginoux, A. Gnanadesikan, C.T. Gordon, S.M. Griffies, R. Gudgel, M.J. Harrison, I.M. Held, R.S. Hemler, L.W. Horowitz, S.A. Klein, T.R. Knutson, P.J. Kushner, A.R. Langenhorst, H.C. Lee, S.J. Lin, J. Lu, S.L. Malyshev, P.C.D. Milly, V. Ramaswamy, J. Russell, M.D. Schwarzkopf, E. Shevliakova, J.J. Sirutis, M.J. Spelman, W.F. Stern, M. Winton, A.T. Wittenberg, B. Wyman, F. Zeng, and R. Zhang. 2006. GFDL's CM2 global coupled climate models. Part I: Formulation and simulation characteristics. Journal of Climate 19(5):643-674.

Fernandez, C., J.Q. Wu, D.K. McCool, and C.O. Stockle. 2003. Estimating water erosion and sediment yield with GIS, RUSLE, and SEDD. Journal of Soil and Water Conservation 58(3):128-136.

Ferro, V., and P. Porto. 1999. A comparative study of rainfall erosivity estimation for southern Italy and southeastern Australia. Hydrological Sciences Journal 44(1):3-23.

Flato, G.M., and G.J. Boer. 2001. Warming asymmetry in climate change simulations. Geophysical Research Letters 28(1):195-198.

Flato, G.M., G.J. Boer, W.G. Lee, N.A. McFarlane, D. Ramsden, M.C. Reader, and A.J. Weaver. 2000. The Canadian Centre for Climate Modelling and Analysis global coupled model and its climate. Climate Dynamics 16(6):451-467.

Flato, G.M., and W.D. Hibler. 1992. Modeling pack ice as a cavitating fluid. Journal of Physical Oceanography 22(6):626-651.

Fry, J.A., G. Xian, S. Jin, J.A. Dewitz, C.G. Homer, L. Yang, C.A. Barnes, N.D. Herold, and J.D. Wickham. 2011. National Land Cover Database for the Conterminous United Sates. Photogrammetric Engineering and Remote Sensing 77(9):859-864.

Gent, P.R., and J.C. McWilliams. 1990. Isopycnal mixing in Ocean Circulation Models. Journal of Physical Oceanography 20(1):150-155.

Gnanadesikan, A., K.W. Dixon, S.M. Griffies, V. Balaji, M. Barreiro, J.A. Beesley, W.F. Cooke, T.L. Delworth, R. Gerdes, M.J. Harrison, I.M. Held, W.J. Hurlin, H.C. Lee, Z. Liang, G. Nong, R.C. Pacanowski, A. Rosati, J. Russell, B.L. Samuels, Q. Song, M.J. Spelman, R.J. Stouffer, C.O. Sweeney, G. Vecchi, M. Winton, A.T. Wittenberg, F. Zeng, R. Zhang, and J.P. Dunne. 2006. GFDL's CM2 global

Figure 6
Mean vulnerability to erosion by (a) eight-digit hydrologic unit code watershed (HUC-8) and (b) hydrologic region

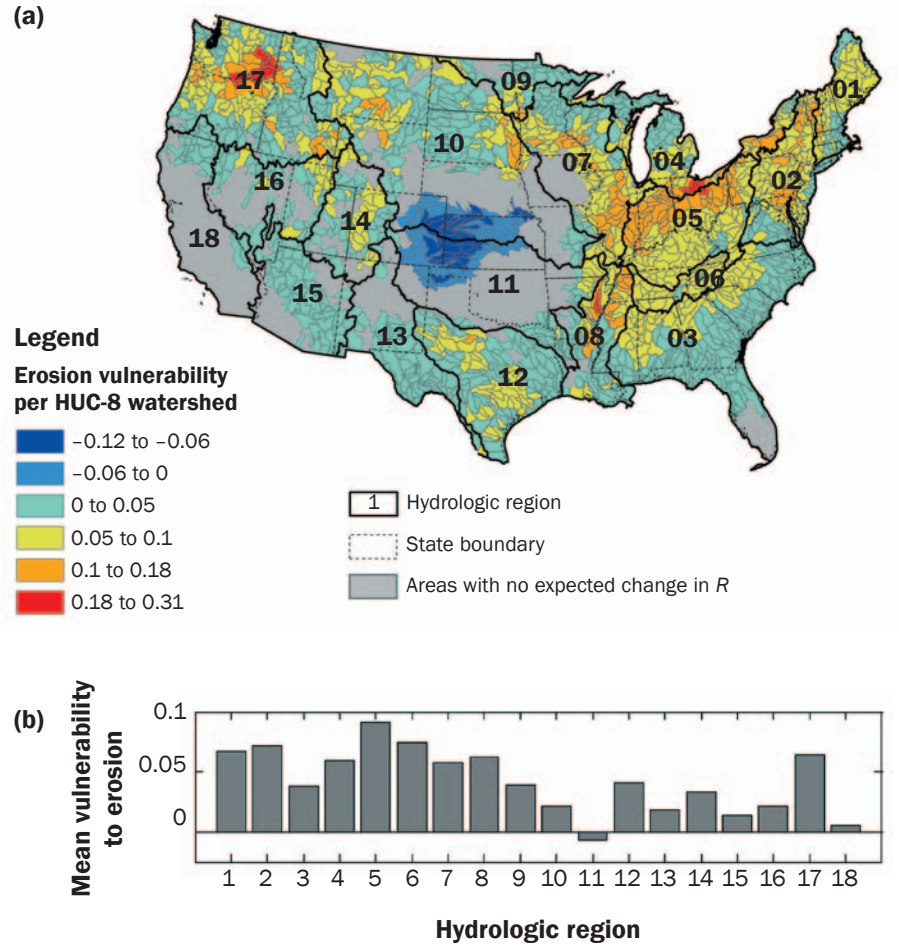

coupled climate models. Part II: The baseline ocean simulation. Journal of Climate 19(5):675-697.

Gordon, C., C. Cooper, C.A. Senior, H. Banks, J.M. Gregory, T.C. Johns, J.F.B. Mitchell, and R.A. Wood. 2000. The simulation of SST, sea ice extents and ocean heat transports in a version of the Hadley Centre coupled model without flux adjustments. Climate Dynamics 16(2-3):147-168.

Intergovernmental Panel on Climate Change (IPCC). 2001. Climate change 2001: Synthesis report. A contribution of working groups I, II, and III to the third assessment report of the Intergovernmental Panel on Climate Change. *In* Anonymous. Cambridge: University Press,

Irvem, A., F. Topaloglu, and V. Uygur. 2007. Estimating spatial distribution of soil loss over Seyhan River Basin in Turkey. Journal of Hydrology 336(1-2):30-37.

Jarvis, A., H. Reuter, A. Nelson, and E. Guevara. 2006. Hole-Filled Seamless SRTM Data V4. International Centre for Tropical Agriculture (CIAT), Cali, Colombia. http://srtm.csi.cgiar.org.

Jiang, Z., S. Su, C. Jing, S. Lin, X. Fei, and J. Wu. 2012. Spatiotemporal dynamics of soil erosion risk for Anji County, China. Stochastic Environmental Research and Risk Assessment 26(6):751-763.

Kemp, P., D. Sear, A. Collins, P. Naden, and I. Jones. 2011. The impacts of fine sediment on riverine fish. Hydrological Processes 25(11):1800-1821.

Kim, S.J., G.M. Flato, and G.J. Boer. 2003. A coupled climate model simulation of the last glacial maximum, Part 2: approach to equilibrium. Climate Dynamics 20(6):635-661.

Kim, S.J., G.M. Flato, G.J. Boer, and N.A. McFarlane. 2002. A coupled climate model simulation of the Last Glacial Maximum, Part 1: transient multi-decadal response. Climate Dynamics 19(5-6):515-537.

Li, Z., W. Liu, X. Zhang, and F. Zheng. 2011. Assessing the site-specific impacts of climate change on hydrology, soil erosion and crop yields in the Loess Plateau of China. Climatic Change 105(1-2):223-242.

Liang, Y.G., S.R. Durrans, and T. Lightsey. 2002. A revised version of pnET-II to simulate the hydrologic cycle in southeastern forested areas. Journal of the American Water Resources Association 38(1):79-89.

Lo, A., S. El-Swaify, E. Dangler, and L. Shinshito. 1985. Effectiveness of EI30 as an erosivity index in Hawaii. *In* Soil Erosion and Conservation, eds. S.A. El-Swaify, W. Moldenhauer, and A. Lo, 384-92. Ankeny, IA: Soil Conservation Society of America.

Loureiro, N.D., and M.D. Coutinho. 2001. A new procedure to estimate the RUSLE EI30 index, based on monthly rainfall data and applied to the Algarve region, Portugal. Journal of Hydrology 250(1-4):12-18.

Maurer, E., L. Brekke, T. Pruit, and P. Duffy. 2007. Fine-resolution climate projections enhance regional climate change impact studies. Transactions of the American Geophysical Union 88(47):504.

Meehl, G., C. Covey, T. Delworth, M. Latif, B. McAvaney, J. Mitchell, R. Stouffer, and K. Taylor. 2007. The WCRP CMIP3 multi-model dataset: A new era in climate change research. Bulletin of the American Meteorological Society 88:1383-1394.

Mikhailova, E.A., R.B. Bryant, S.J. Schwager, and S.D. Smith. 1997. Predicting rainfall erosivity in Honduras. Soil Science Society of America Journal 61(1):273-279.

Millward, A.A., and J.E. Mersey. 1999. Adapting the RUSLE to model soil erosion potential in a mountainous tropical watershed. Catena 38(2):109-129.

Nearing, M.A. 2001. Potential changes in rainfall erosivity in the US with climate change during the 21(st) century. Journal of Soil and Water Conservation 56(3):229-232.

Oliveira, P.T.S., D.B.B. Rodrigues, T.A. Sobrinho, D.F. de Carvalho, and E. Panachuki. 2012. Spatial Variability of the Rainfall Erosive Potential in the State of Mato Grosso do Sul, Brazil. Engenharia Agricola 32(1):69-79.

Ozsoy, G., E. Aksoy, M.S. Dirim, and Z. Tumsavas. 2012. Determination of soil erosion risk in the Mustafakemalpasa River Basin, Turkey, using the Revised Universal Soil Loss Equation, Geographic Information System, and Remote Sensing. Environmental management 50(4):679-694.

Pope, V.D., M.L. Gallani, P.R. Rowntree, and R.A. Stratton. 2000. The impact of new physical parametrizations in the Hadley Centre climate model: HadAM3. Climate Dynamics 16(2-3):123-146.

Pruski, F.F., and M.A. Nearing. 2002. Runoff and soil-loss responses to changes in precipitation: A computer simulation study. Journal of Soil and Water Conservation 57(1):7-16.

Renard, K.G., G.R. Foster, G.A. Weesies, and J.P. Porter. 1991. Rusle - Revised Universal Soil Loss Equation. Journal of Soil and Water Conservation 46(1):30-33.

Renard, K.G., and J.R. Freimund. 1994. Using monthly precipitation data to estimate the R-Factor in the Revised Usle. Journal of Hydrology 157(1-4):287-306.

Roose, E. 1977. Application of the universal soil erosion loss equation of Wischmeier and Smith in West Africa. *In* Soil Conservation and Management in the Humid Tropics,

eds. D. Greenland and R. Lai, 166-177. Chichester: John Wiley & Sons.

Schwede, D.B., R.L. Dennis, and M.A. Bitz. 2009. The Watershed Deposition Tool: A Tool for Incorporating Atmospheric Deposition in Water-Quality Analyses (1). Journal of the American Water Resources Association 45(4):973–985.

Sepaskhah, A.P., and P. Sarkhosh. 2005. Estimating storm erosion index in southern region of IR Iran. Iranian Journal of Science and Technology Transaction B-Engineering 29(B3):237-248.

Stocking, M.A., and H.A. Elwell. 1976. Rainfall erosivity over Rhodesia. Transactions of the Institute of British Geographers 1(2):231-245.

Stouffer, R.J., A.J. Broccoli, T.L. Delworth, K.W. Dixon, R. Gudgel, I. Held, R. Hemler, T. Knutson, H.C. Lee, M.D. Schwarzkopf, B. Soden, M.J. Spelman, M. Winton, and F. Zeng. 2006. GFDL's CM2 global coupled climate models. Part IV: Idealized climate response. Journal of Climate 19(5):723-740.

Sun, G., P. Caldwell, A. Noormets, S.G. McNulty, E. Cohen, J.M. Myers, J. Domec, E. Treasure, Q. Mu, J. Xiao, R. John, and J. Chen. 2011. Upscaling key ecosystem functions across the conterminous United States by a water-centric ecosystem model. Journal of Geophysical Research-Biogeosciences 116(G00J05):G00J05.

Sun, G., S.G. McNulty, J.A.M. Myers, and E.C. Cohen. 2008. Impacts of multiple stresses on water demand and supply across the southeastern United States. Journal of the American Water Resources Association 44(6):1441-1457.

Theobald, D.M., S.J. Goetz, J.B. Norman, and P. Jantz. 2009. Watersheds at risk to increased impervious surface cover in the conterminous United States. Journal of Hydrologic Engineering 14(4):362-368.

Trenberth, K.E., P. Jones, P. Ambenje, R. Bojariu, D. Easterling, A. Klein Tank, D. Parker, F. Rahimzadeh, J. Renwick, M. Rusticucci, B. Soden, and P. Zhai. 2007. Observations: Surface and Atmospheric Climate Change. *In* Climate Change 2007: The Physical Science Basis. Contribution of Working Group I to the Fourth Assessment Report of the Intergovernmental Panel on Climate Change, eds. S. Solomon , D. Qin, M. Manning, Z. Chen, M. Marquis, K. Averyt, M. Tignor, and H. Miller. UK and New York: NY, USA. Cambridge University Press.

Van Rompaey, A., G. Verstraeten, K. Van Oost, G. Govers, and J. Poesen. 2001. Modelling mean annual sediment yield using a distributed approach. Earth Surface Processes and Landforms 26(11):1221-1236.

Waters, T. 1995. Sediment in streams: Sources, biological effects, and control. Bethesda, MD: American Fisheries Society Monograph 7.

Wischmeier, W., and D. Smith. 1978. Predicting rainfall erosion losses: A guide to conservation planning. Washington, DC: US Government Printing Office. Agricultural Handbook No. 537.

Wittenberg, A.T., A. Rosati, N.C. Lau, and J.J. Ploshay. 2006. GFDL's CM2 global coupled climate models. Part III: Tropical pacific climate and ENSO. Journal of Climate 19(5):698-722.

Wolock, D. 1997. STATSGO soil characteristics for the conterminous United States. Lawrence, KS: US Geological Survey.

Wood, P., and P. Armitage. 1997. Biological effects of fine sediment in the lotic environment. Environmental Management 21(2):203-217.

Wood, R.A., A.B. Keen, J.F.B. Mitchell, and J.M. Gregory. 1999. Changing spatial structure of the thermohaline circulation in response to atmospheric CO (2) forcing in a climate model. Nature 399(6736):572-575.

Wright, C.K., and M.C. Wimberly. 2013. Recent land use change in the Western Corn Belt threatens grasslands and wetlands. *In* proceedings of the National Academy of Sciences of the United States of America 110(10):4134-4139.

Yang, D.W., S. Kanae, T. Oki, T. Koike, and K. Musiake. 2003. Global potential soil erosion with reference to land use and climate changes. Hydrological Processes 17(14):2913–2928.

Zhang, X. 2012. Cropping and tillage systems effects on soil erosion under climate change in Oklahoma. Soil Science Society of America Journal 76(5):1789-1797.

Zhang, X.C., and W.Z. Liu. 2005. Simulating potential response of hydrology, soil erosion, and crop productivity to climate change in Changwu tableland region on the Loess Plateau of China. Agricultural and Forest Meteorology 131(3-4).

Zhang, Y., M. Hernandez, E. Anson, M.A. Nearing, H. Wei, J.J. Stone, and R. Heilman. 2012. Modeling climate change effects on runoff and soil erosion in southeastern Arizona rangelands and implications for mitigation with conservation practices. Journal of Soil and Water Conservation 67(5):390-405 doi:10.2489/jswc.67.5.390.

Zhang, Y.G., M.A. Nearing, X.C. Zhang, Y. Xie, and H. Wei. 2010. Projected rainfall erosivity changes under climate change from multimodel and multiscenario projections in Northeast China. Journal of Hydrology. 384(1-2):97-106.